JACS
JOURNAL OF THE AMERICAN CHEMICAL SOCIETY
pubs.acs.org/JACS

Article

Monodentate σ-Accepting Boron-Based Ligands Bearing Square-Planar Ni(0) Centers

Yutaka Mondori, Yasuhiro Yamauchi, Takahiro Kawakita, Sensuke Ogoshi, Yuta Uetake,* Yasuo Takeichi, Hidehiro Sakurai, and Yoichi Hoshimoto*

Cite This: J. Am. Chem. Soc. 2025, 147, 8326–8335

Read Online

ACCESS | Metrics & More | Article Recommendations | Supporting Information

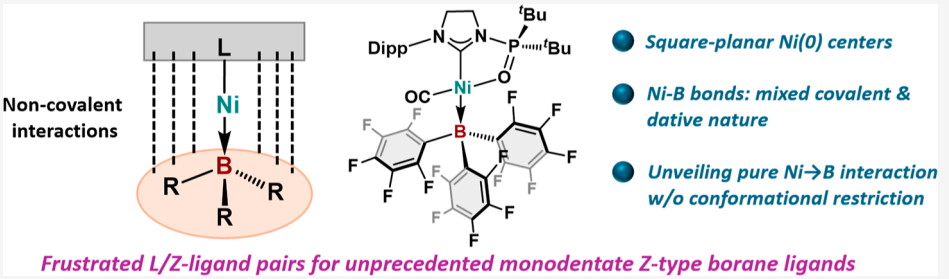

ABSTRACT: Transition metals are known to work as electron donors toward electron-accepting heavier-group-13 elements (Al, Ga, and In), called Z-type ligands. However, complexes with boron-based Z-type ligands are stable only in the presence of additional coordination units (the so-called "supported-ligand" strategy). Here, we report the synthesis and characterization of square-planar Ni(0) complexes that bear tris(perfluoroaryl)boranes as monodentate Z-type ligands, even though such coordination geometry has been traditionally associated with Ni(II) species based on the well-established ligand-field theory. A combined theoretical and experimental approach revealed a mixed covalent/dative character for the Ni−B bonds. This strategy uses frustrated L/Z-ligand pairs that combine sterically encumbered electron-donating (L-type) and electron-accepting ligands to form noncovalent interactions over L−M−Z units to achieve unprecedented low-valent transition metal species with monodentate Z-type ligands.

INTRODUCTION

The concept of electron acceptors (i.e., Lewis acids; LAs) and donors (i.e., Lewis bases; LBs) has played a pivotal role in understanding chemical bonds between molecular fragments in various fields of chemistry (Figure 1a, top).[1] As a representative example, transition metal complexes, which are employed in the synthesis of pharmaceuticals, polymers, and commodities,[2,3] are constructed via the sharing of electrons between transition metals (TM) as LAs and ligands as LBs. Such TM ← LB interactions involve the transfer of electron(s) from an electron-occupied orbital (e.g., s, p, and their hybridized orbitals) in the LB to an empty d-orbital of TM (Figure 1a, middle); the arrow indicates the direction of the donor-to-acceptor-transfer of electrons. TM can simultaneously act as an electron donor via so-called back-donation when adequate orbital(s) in the ligands, such as antibonding σ* and π* orbitals, are available to accept electrons from the filled d-orbital in TM, leading to the formation of TM ⇄ LB bonds.[4] Additionally, electron donation from the filled d-orbitals in TM to empty p orbitals of main-group LAs (i.e., TM → LA) has also been known since the 1960s, although examples remain limited (Figure 1a, bottom).[5−10] These Lewis-acidic σ-accepting ligands are often referred to as Z-type ligands (formal two-electron acceptors) based on the number of electrons donated/accepted to/from TM, as proposed by Green[11] and Parkin,[9] while formal one- and two-electron donors are known as X- and L-types, respectively.

Trivalent group-13 molecules, i.e., EX_3 (E = B, Al, Ga, In), are typical LAs, as the empty p orbitals on the central E atom can accept electrons from various LBs, including main-group[12,13] and transition metals (Figure 1b). Since Burlitch, Hughes and co-workers crystallographically identified the presence of the Fe → Al bonding interaction in $[Et_4N][Fe(AlPh_3)(cyclopentadienyl)(CO)_2]$,[14] EX_3 ligands have been employed as monodentate, unsupported Z-type ligands to accept electrons from a variety of transition metals.[5,7,10,15] However, the formation of the unsupported TM → BX_3 interaction remains elusive due to the absence of crystallographical evidence, even though such a bonding situation has often been proposed based on experimental results using NMR and/or IR spectroscopy techniques.[5,7,16,17] In this context,

Received: November 10, 2024
Revised: February 10, 2025
Accepted: February 18, 2025
Published: February 28, 2025

https://doi.org/10.1021/jacs.4c15892
J. Am. Chem. Soc. 2025, 147, 8326−8335

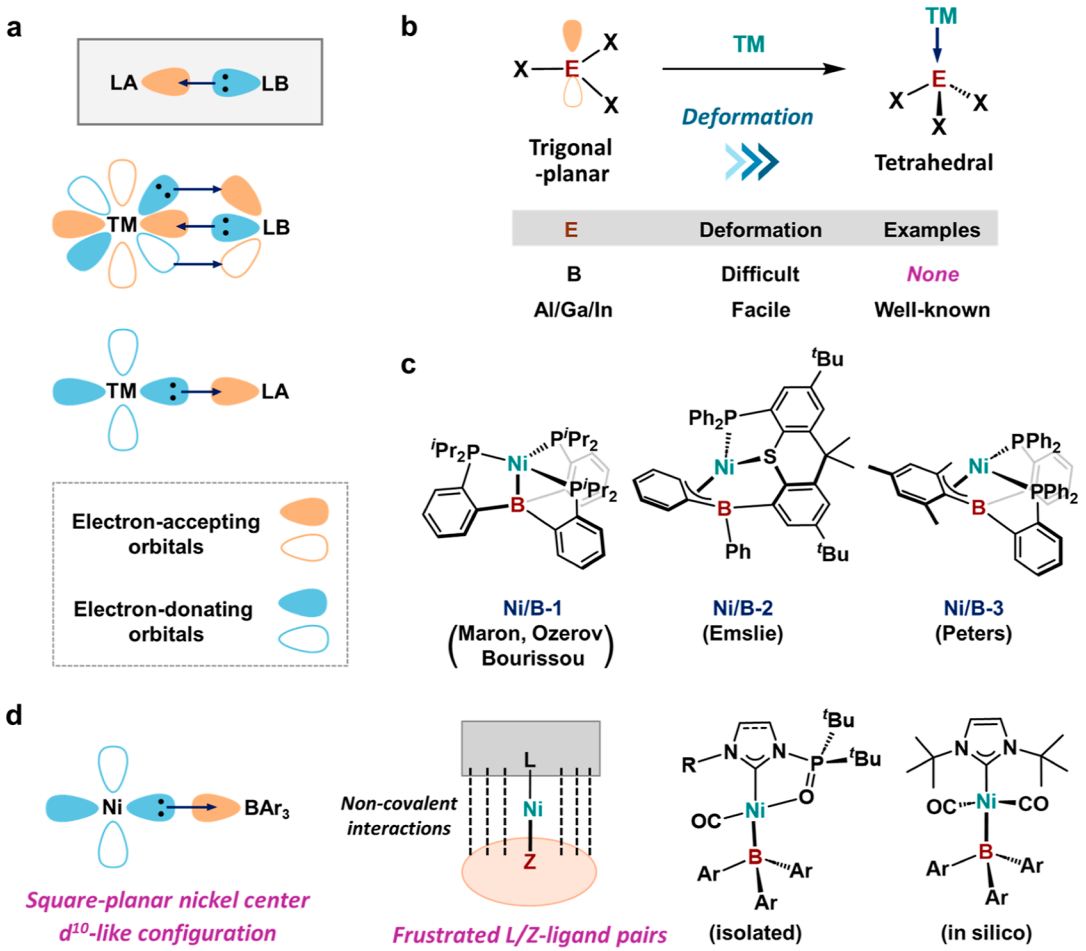

Figure 1. Concept of electron acceptors and donors. (a) A simplified representation of complexation between Lewis acids (LAs) and Lewis bases (LBs) and the related orbitals. (b) Coordination of transition metals (TM) to trivalent group-13 species. (c) Pioneering examples of Ni complexes that bear L_nZ-type borane ligands. (d) A strategy for monodentate Z-type borane ligands based on frustrated L/Z-ligand pairs (this work).

Burlitch, Hughes, and co-workers proposed, based on IR and NMR analyses, the formation of Fe → BPh_3 interactions after the reaction between $[NEt_4][(\eta^5\text{-cyclopentadienyl})Fe(CO)_2]$ and BPh_3;[17] however, even though the formation of a four-coordinated boron species was suggested, such spectroscopic analyses still remain questionable when discussing the existence of TM → BX_3 interactions, as we demonstrate in this manuscript (see our results on e.g., **2a**, **6a**, and **7g**). Remarkably, Campos and co-workers have recently reported that a Rh(I) complex bearing $HB(C_6F_5)_2$ includes a bonding interaction between the Rh center and the B−H bond, and proposed that this complex may be potentially described as a transition metal complex bearing an unsupported borane ligand.[18] Based on our experience in custom-tailoring the Lewis acidity of triarylboranes (X = aryl)[19−21] and the report of Frenking[22] and co-workers, we are convinced that the striking differences in the reactivity of BX_3 and its heavier analogues can be explained by the energetic penalty for the geometric deformation (E_{def}) from the trigonal-planar to the tetrahedral conformation via the formation of TM−EX_3 bonds (Figure 1b). In fact, the E_{def} values for BX_3 (X = halogen, alkyl, aryl) have been predicted to be at least twice those of the corresponding Al, Ga, and In analogues when triethylphosphine oxide was used as a model LB.[23] One strategy to compensate for this high E_{def} and to stabilize the tetrahedral TM−BX_3 motif is the use of boranes that are equipped with additional L-type coordination units such as phosphines. In 1999, Hill and co-workers reported the synthesis and identification of several transition metal complexes that bear $B(mt)_3$ (mt = 2-sulfanyl-1-methylimidazole) as a multidentate L_3Z-type ligand.[24,25] However, these authors also pointed out the significant contribution of an imidazole-coordinated σ-boryl canonical form (an L_2X_2-type) of the $B(mt)_3$ ligand; thus, a careful discussion of the nature of TM−borane bonds is required.[26,27] Later, Bourissou and co-workers successfully demonstrated that triarylboranes that bear di- or triphosphanyl moieties can serve as an adequate platform to construct supported TM−borane complexes[6] such as **Ni/B-1**[28] (Figure 1c). Moreover, **Ni/B-2** and **Ni/B-3** have been synthesized by Emslie[29] and Peters,[30] respectively, and both have been proposed to include an η^3-BCC coordination of an aryl borane unit to the nickel center. These pioneering results demonstrated that BX_3 has sufficient electrophilicity to accept electrons donated from TM if the energetic penalty in the geometry deformation is effectively compensated. Nevertheless, an approach to successfully realize unsupported, monodentate Z-type borane ligands has remained elusive so far.

Herein, we report the synthesis of square-planar nickel(0) complexes that bear boranes as monodentate Z-type ligands via L-to-Z ligand substitution on the nickel(0) carbonyl complexes (Figure 1d). We found that the combination of sterically

https://doi.org/10.1021/jacs.4c15892
J. Am. Chem. Soc. 2025, 147, 8326−8335

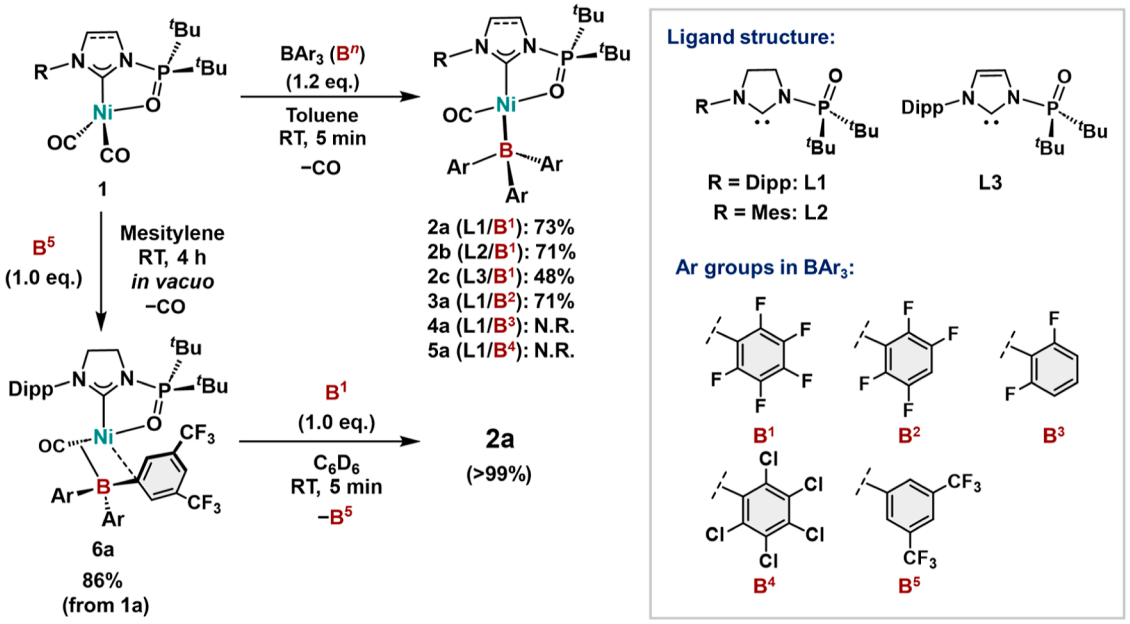

Figure 2. Reaction between Ni-carbonyl complexes and triarylboranes. The isolated yield is shown with the NMR yield in parentheses; N.R.: no reaction; Dipp: 2,6-diisopropylphenyl; Mes: mesityl.

encumbered *N*-heterocyclic carbenes (NHCs) as L-type ligands and tris(perfluoroaryl)boranes ($\mathbf{B}^n$) as Z-type ligands (i.e., frustrated L/Z-ligand pairs, named in analogy to the concept of frustrated Lewis pairs, FLPs)[31,32] is critical to generate these elusive species. The participation of multiple noncovalent interactions (NCI) over the NHC−TM−$\mathbf{B}^n$ units is discussed based on a systematic theoretical analysis.

RESULTS AND DISCUSSION

We have reported the formation of heterobimetallic Ni/Al complexes that bear *N*-phosphine-oxide-substituted imidazolinylidene **L1** (Figure 2) as a bridging ligand via the $Al(C_6F_5)_3$-induced rotation of the *N*-phosphinoyl moieties in (κ-*C*,*O*-**L1**)Ni(CO)$_2$ (**1a**).[33] In the present study, we first attempted to extend this strategy, i.e., the Lewis acid-mediated reversible modulation of the local environment around the metal center, by exploring the reaction between **1a** and $B(C_6F_5)_3$ ($\mathbf{B}^1$), i.e., the boron analogue of $Al(C_6F_5)_3$, with the expectation of forming the corresponding Ni/B bimetallic complex. However, upon dissociation of CO, we unexpectedly obtained (κ-*C*,*O*-**L1**)Ni(CO)($\mathbf{B}^1$) (**2a**), which was isolated in 73% yield (Figure 2). In the ^{11}B NMR spectrum of **2a** in α,α,α-trifluorotoluene (TFT), the resonance of the $\mathbf{B}^1$ unit is observed at δ_B −10.3, which represents a significant upfield shift compared to that of free $\mathbf{B}^1$ (δ_B 59.9) and suggests the formation of a four-coordinated boron species. For comparison, complexes bearing phosphine-boranes such as **Ni/B-1** display downfield-shifted resonances (δ_B 15−30),[28−30] highlighting the difference between the present unsupported Z-type systems and the hitherto reported supported systems. We have also isolated (κ-*C*,*O*-**L2**)Ni(CO)($\mathbf{B}^1$) (**2b**) and (κ-*C*,*O*-**L3**)Ni(CO)($\mathbf{B}^1$) (**2c**) in 71% and 48% yield, respectively, via L-to-Z ligand substitution. Under an inert-gas atmosphere at −30 °C, crystalline samples of **2a**−**2c** are stable for at least several months. These complexes are nearly insoluble in nonpolar hydrocarbons such as *n*-pentane and *n*-hexane, slightly soluble in aromatic hydrocarbons such as benzene and toluene, and fully soluble in TFT. These nickel−borane complexes slowly decompose into unidentified products once dissolved in TFT (e.g., **2a**: $t_{1/2}$ = 615 min at 23 °C).

To investigate which properties are essential to the ability of triarylboranes to induce the Ni → BAr_3 interaction, we treated **1a** with $B(2,3,5,6\text{-}F_4C_6H)_3$ ($\mathbf{B}^2$) and $B(2,6\text{-}F_2C_6H_3)_3$ ($\mathbf{B}^3$); the Lewis acidity of these boranes decreases in the order $\mathbf{B}^1 > \mathbf{B}^2 > \mathbf{B}^3$ (for details of the Lewis acidity of $\mathbf{B}^1$−$\mathbf{B}^5$ toward $Et_3P{=}O$, see Table S1).[34] Interestingly, (κ-*C*,*O*-**L1**)Ni(CO)($\mathbf{B}^2$) (**3a**) was obtained in 71% yield; however, no reaction proceeded when $\mathbf{B}^3$ was employed, representing a plausible threshold of Lewis acidity below which the reactions between **1a** and boranes cannot proceed. This hypothesis is consistent with the fact that no reaction occurred using $B(C_6Cl_5)_3$ ($\mathbf{B}^4$), which exhibits lower Lewis acidity but higher electrophilicity than $\mathbf{B}^1$.[35] We then explored the effect of the *ortho*-F atoms in the *B*-aryl groups by using $B(3,5\text{-}(CF_3)_2C_6H_3)_3$ ($\mathbf{B}^5$). $\mathbf{B}^5$ has been reported to exhibit higher Lewis acidity than $\mathbf{B}^1$ due to the electron-withdrawing nature of the *meta*-CF_3 groups as well as the reduced intramolecular repulsion between *ortho*-H atoms in the tetrahedral four-coordinated boron unit.[36] Although a change in the NMR spectra was virtually negligible when **1a** and $\mathbf{B}^5$ were mixed under ambient conditions, nickel complex **6a** was isolated in 86% yield when the reaction mixture was stirred under reduced pressure to promote the removal of CO (Figure 2). Notably, in stark contrast to **2a**−**c** and **3a**, no resonance was observed in the ^{11}B NMR spectrum of **6a**. We therefore concluded that the corresponding Ni → $\mathbf{B}^5$ interaction does not manifest in this complex. Based on the results of the single-crystal X-ray diffraction (SC-XRD) and density functional theory (DFT) calculation analyses (vide infra), we concluded that in **6a**, interactions between the Ni−CO bond and the boron atom, as well as between the Ni atom and one of the *ipso*-C atoms in the aryl group occur. Thus, $\mathbf{B}^5$ does not act as a typical Z-type ligand under the applied reaction conditions, although the observed bonding situations are nearly identical to those found in **Ni/B-2** and **Ni/B-3** (Figure S20). We subsequently used **6a** as a precursor for preparing Ni−borane complexes via the borane−exchange

https://doi.org/10.1021/jacs.4c15892
J. Am. Chem. Soc. 2025, 147, 8326−8335

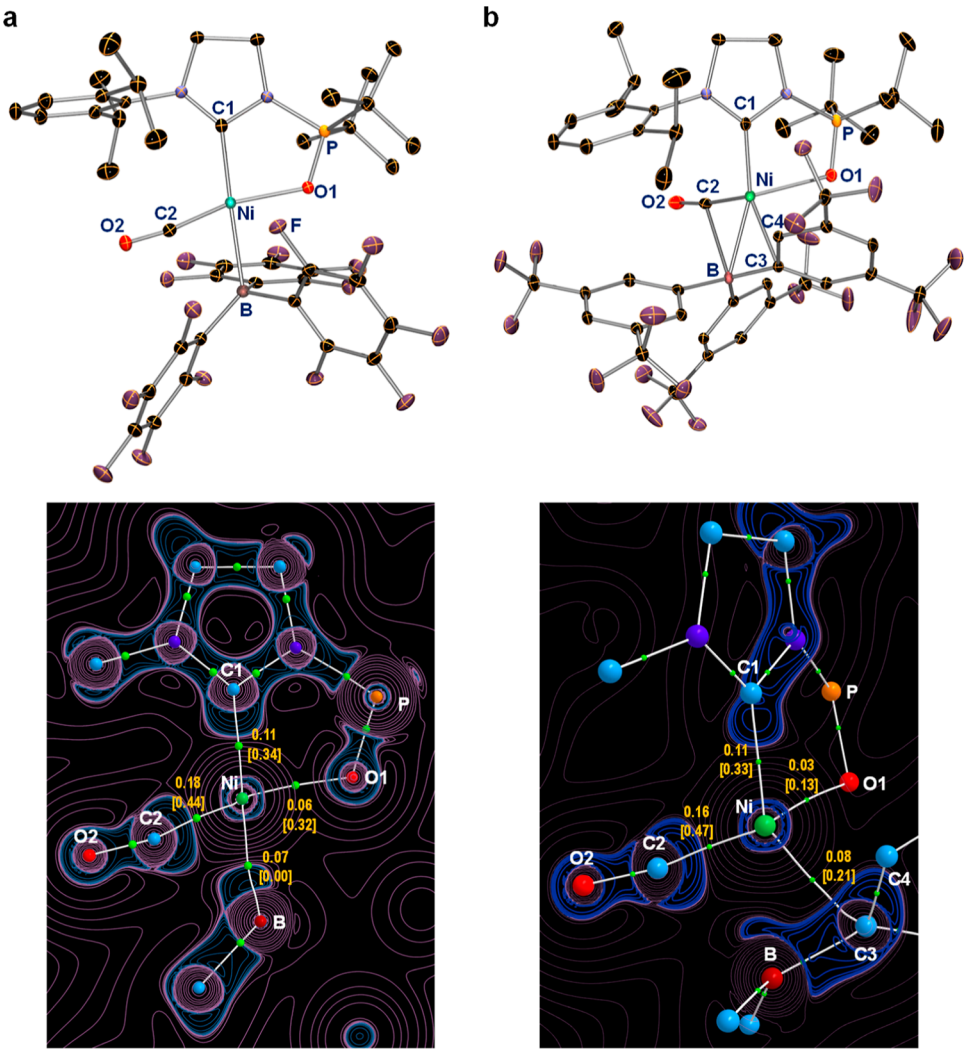

Figure 3. Molecular structures and electron densities for (a) **2a** and (b) **6a**. Each structure was obtained from the corresponding SC-XRD analysis. The quantum theory of AIM bond paths (white lines) and bond critical points (BCPs, green dots) are also shown with overlaid contour plots of $\nabla^2\rho$ ($e \times r_{Bohr}^{-5}$) through the plane defined by the C2, Ni, and B atoms ($\nabla^2\rho < 0$ shown in blue; $\nabla^2\rho > 0$ shown in red). The AIM methods used the SCF electron density calculated at the PBE0-D3BJ/Def2-TZVPD//M06L/Def2-SVPD(Ni,O,F), Def2-SVP(others) level. Electron densities (ρ in $e \times r_{Bohr}^{-3}$) at selected BCPs are given. Values of $\nabla^2\rho$ are also given in parentheses. Selected bond lengths (Å) for **2a**: Ni−C1 1.976(1), Ni−C2 1.697(1), Ni−B 2.245(1), Ni−O1 1.9916(9), C2−O2 1.154(1), Ni···F 2.7450(9); **6a**: Ni−C1 1.946(2), Ni−C2 1.735(3), Ni−B 2.267(4), Ni−C3 2.110(2), Ni···C4 2.238(2), Ni−O1 2.320(2), C2−B 2.373(4), C2−O2 1.146(3).

reaction. The quantitative formation of **2a** was confirmed when **6a** was treated with **B**[1]. These results demonstrate the role of the *ortho*-F atoms of the Z-type tris(perfluoroaryl)borane ligands in the formation of the Ni → **B**″ interactions in **2a**−**2c** and **3a**.

Complexes **2a**−**c**, **3a**, and **6a** were unambiguously characterized using SC-XRD analysis. Selected geometric parameters are summarized and compared with the reported parameters in **Ni/B-1**, **Ni/B-2**, and **Ni/B-3** in Table S2. The molecular structures of **2a** and **6a** are shown in Figure 3a,b, respectively, together with a topological analysis of the electron density based on the atoms-in-molecules (AIM) theory. The Ni−B bond length in **2a** (2.245(1) Å) falls within the expected bond-length range for supported TM−borane complexes[7] (ca. 2.05−2.90 Å) but is clearly longer than those in **Ni/B-1** (2.168(2) Å) and **Ni/B-3** (2.1543(9) Å). Notably, the interatomic distance between the Ni and B atoms in **6a** (2.267(4) Å) is nearly identical to that in **2a**, despite the fact that the NMR analyses of **6a** do not support the formation of a four-coordinated boron species (vide supra). Furthermore, in the case of **2a**, a bond critical point (BCP) was confirmed between the Ni and B atoms (electron density ρ = 0.07 [$e \times r_{Bohr}^{-3}$]; Laplacian of electron density $\nabla^2\rho$ = 0.00 [$e \times r_{Bohr}^{-5}$]) (Figure 3a, bottom) in AIM analysis. These results suggest that the Ni−B bond in **2a** possesses mixed covalent/dative bond properties. On the other hand, a corresponding BCP is not observed in **6a**, again suggesting the absence of a significant Ni → B interaction (Figure 3b, bottom). These results suggest that the existence of TM → B bonding interactions should not be discussed based on the interatomic distance between the TM and B atoms. A natural bond orbital (NBO) analysis also highlights characteristic interactions involved in **2a** (Figure S23). Donor−acceptor interactions between the Ni and B atoms ($E^{(2)}$ = +26.9 kcal mol^{-1}) and carbonyl C2 and B atoms ($E^{(2)}$ = +57.6 kcal mol^{-1}) were confirmed in **2a** based on second-order-perturbation-theory analysis, suggesting a three-center four-electron bond among the Ni, B, and C2 atoms. It should also be noted here that the Ni → BX_3 interaction can

https://doi.org/10.1021/jacs.4c15892
J. Am. Chem. Soc. 2025, 147, 8326−8335

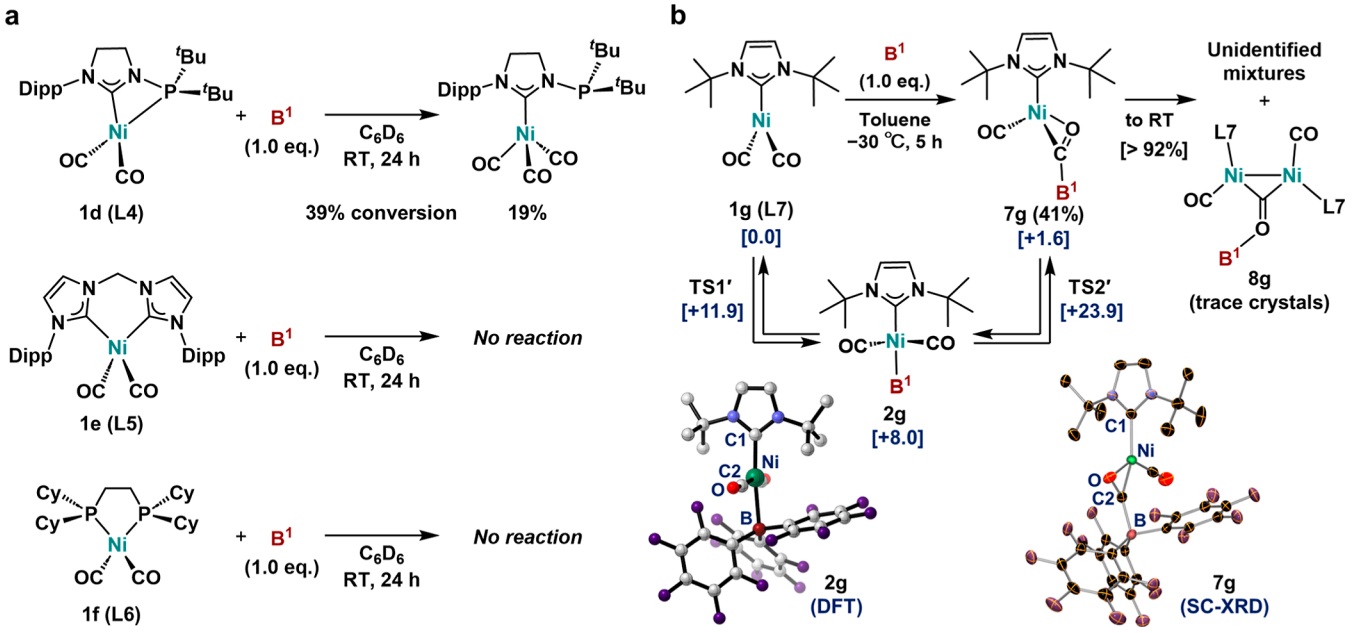

Figure 4. Effect of ligands. (a) Reaction with **1d**−**1f**. (b) Reaction with **1g**. The conversion of **1g** through the transformation of **7g** is shown in square brackets. The gas-phase optimized structure of **2g** and the SC-XRD structure of **7g** (except hydrogen atoms; thermal ellipsoids at 30% probability) are also shown. Selected bond lengths (Å) for **2g**: Ni−C1 2.00, Ni−C2 1.82, Ni−B 2.43, C2−O 1.15; **7g**: Ni−C1 1.976(4), Ni−O 1.966(3), Ni−C2 1.843(4), C2−O 1.207(5), C2−B 1.639(5).

be interpreted in terms of a reversed bonding situation compared to the TM ← BL_nX_{3-n} (n = 1−2) interaction in borylene-coordinated transition metal complexes, wherein TMs and borylenes play the roles of LAs and LBs, respectively.[37,38]

Although the AIM analysis does not support the existence of a BCP between the C2 and B atoms in **2a**, the unusual topology of $\nabla^2\rho$ between the C2 and B atoms (Figure 3a, bottom) is consistent with a partial contribution of the C2 → B electron transfer. Similarly, the corresponding C2 → B interaction ($E^{(2)}$ = +49.0 kcal mol^{-1}) in **6a** was also confirmed by the NBO analysis, while the Ni → B interaction ($E^{(2)}$ = +14.5 kcal mol^{-1}) was found to be less significant (Figure S25). Based on these results, we conclude that the coordination of the Ni−C2 bond to the B atom is a key feature for understanding the connection between the Ni(**L***m*)(CO) and **B***ⁿ* (n = 1 and 5, m = 1−3) units, as seen in **6a**. When *ortho*-F atoms are involved in **B***ⁿ*, the Ni → B interaction tends to become predominant, affording complexes **2a**−**c** with monodentate Z-type borane ligands. Indeed, the AIM analysis confirmed the participation of an NCI between the Ni center and one of the *ortho*-F atoms in the **B**^{1} unit (interatomic Ni···F distance: 2.7450(9) Å; determined by SC-XRD). The corresponding Ni···F NCIs were also observed in **2c** (2.688(49) Å) and **3a** (2.642(62) Å), whereas **2b**, which bears *N*-mesityl-substituted **L2**, can not be expected to include the interaction between Ni and F atoms (the distance between Ni and the nearest F atoms is 2.948(1) Å). Instead, one of the *ipso*-carbon atoms (C_{ip}) in the *B*-C_6F_5 groups of **2b** closely approaches the Ni center at 2.529(1) Å, which is, however, still longer than those found in **Ni/B-2** (2.018(3) Å)[29] and **Ni/B-3** (2.0750(7) Å).[30] A BCP is found between these two atoms in **2a** (ρ = 0.02 [$e \times r_{Bohr}^{-3}$]; $\nabla^2\rho$ = 0.09 [$e \times r_{Bohr}^{-5}$]; δ(NilF) = 0.10), suggesting that this Ni···F interaction is significantly weaker than e.g., Ni−O1 (ρ = 0.06 [$e \times r_{Bohr}^{-3}$]; $\nabla^2\rho$ = 0.32 [$e \times r_{Bohr}^{-5}$]; δ(NilO1) = 0.34) and Ni−C1 (ρ = 0.11 [$e \times r_{Bohr}^{-3}$]; $\nabla^2\rho$ = 0.34 [$e \times r_{Bohr}^{-5}$]; δ(NilC1) = 0.71) interactions, wherein δ(XlY) values show the average number of electrons shared at a BCP between X and Y atoms. In addition, all *ortho*-F atoms in **2a** are observed at nearly identical shifts in the ^{19}F NMR analysis (δ_F −137 ∼ −122 at −28 °C), suggesting a labile and exchangeable nature of the Ni···F NCIs in solution. Moreover, multiple NCIs are simultaneously observed between the **L1** and **B**^{1} ligands over the Ni atoms in **2a**. We think that these NCIs are not individually essential for the stability of the Ni−borane complexes but rather work cooperatively with other weak interactions.

The geometry around the Ni centers in **2a**−**c** and **3a** was evaluated based on the value of τ_M [$\tau_M = \{360 - (\alpha + \beta)\}/141 \times \beta/\alpha$, where α and β are the largest and second-largest L−M−L angles obtained from their SC-XRD analyses].[39] A τ_M value approaching 0 indicates that M adopts an ideal square-planar geometry, while a value approaching 1 corresponds to an ideal tetrahedral geometry. The Ni centers in **2a**−**c** and **3a** were found to adopt a distorted square-planar geometry with τ_{Ni} values of 0.10−0.16, as has often been found for low-spin Ni(II) complexes; however, we eventually concluded that the electronic state of the Ni center in **2a** would be close to Ni(0) (vide infra) (Figure 6). For the geometry around the boron center, as expected, distorted tetrahedral structures (τ_B = 0.7−0.8) were confirmed in **2a**−**c** and **3a**, while the B atom in **6a** retains a rather planar geometry (sum of C−B−C angles = 353.8°, see also results of the tetrahedral characters [THC(B)] in Table S2).

To further confirm the prerequisite factors for the monodentate Z-type coordination of tris(perfluoroaryl)-boranes, we carried out control experiments using **B**^{1} and nickel carbonyl complexes **1d**−**1f**, which bear **L4**−**L6** (Figure 4a); however, we did not observe the formation of the corresponding Ni−**B**^{1} complex under the applied conditions. In fact, the reaction between *N*-phosphanyl-substituted **1d** and

https://doi.org/10.1021/jacs.4c15892
J. Am. Chem. Soc. 2025, 147, 8326−8335

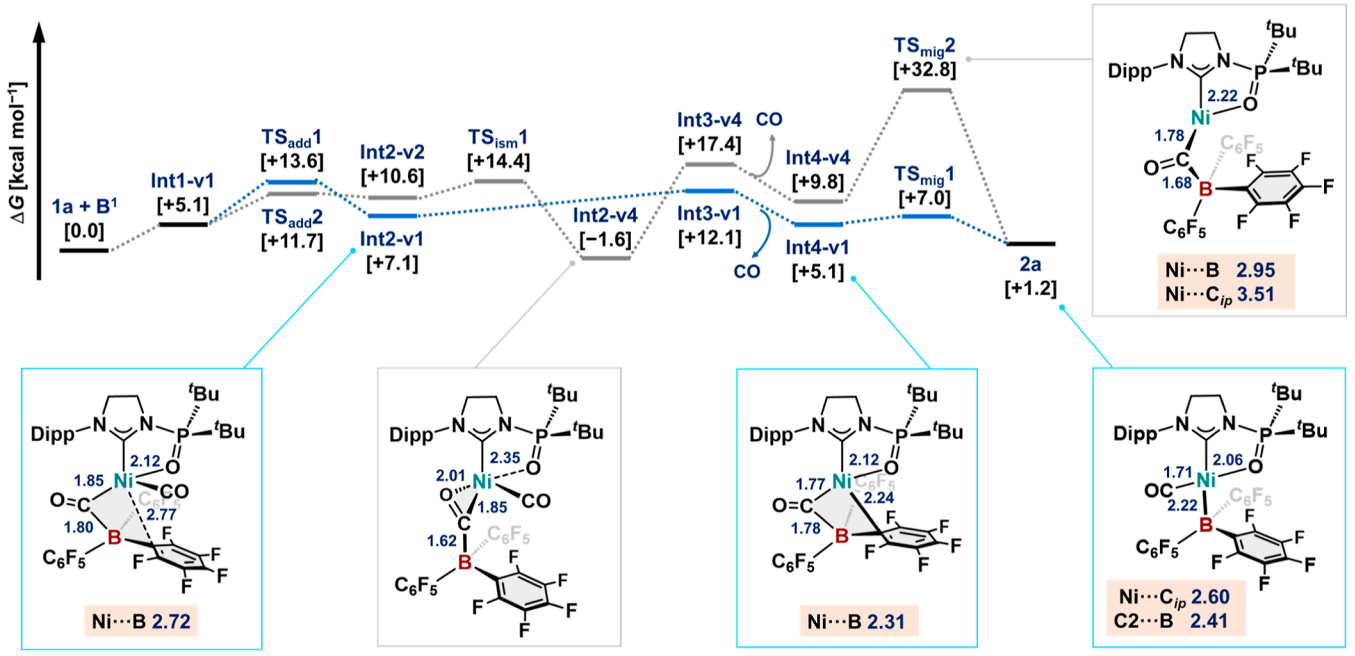

Figure 5. Plausible mechanisms for the formation of **2a**. Relative Gibbs free energies (kcal mol^{-1}) with respect to [**1a** + **B^1**] (0.0 kcal mol^{-1}) are shown, calculated at the PBE0-D3BJ/Def2-TZVPD//M06L/Def2-SVPD(Ni,F,O), Def2-SVP(others) level. Parts of the molecular structures for the selected compounds are also shown with selected bond lengths (Å).

B^1 resulted in the formation of (κ-*C*-**L4**)Ni(CO)$_3$ in 19% yield through **B^1**-induced disproportionation of the CO ligands in **1d**, while other nickel carbonyl species were not identified by ^{31}P and ^{19}F NMR analyses. Thus, the *N*-phosphinoyl oxygen atom in **L1** plays a role in stabilizing **2a** as an isolable species. No reaction took place when **1e** and **1f**, which bear **L5** and **L6**, respectively, were employed. We then turned our attention to **1g**, which bears 1,3-di-*tert*-butylimidazol-2-ylidene **L7**, as it can generate an FLP species with **B^1** (Figure 4b).[40,41] We confirmed the generation of an equilibrium mixture including **1g** (56%) and **7g** (41%) at −30 °C after a period of 5 h. The characterization of **7g** was accomplished based on NMR and SC-XRD analyses, which clearly confirmed the presence of the Ni(μ-η^1,η^2-CO)B unit. The resonance for the corresponding four-coordinated boron moiety was observed at δ_B −14.2 in the ^{11}B NMR spectrum, a shift that is comparable to that reported for the four-coordinated boron complex [Cp$_2$Ti(THF-d_8)(μ-η^1,η^2-CO)**B^1**][42] (Cp = cyclopentadienyl) (δ_B −11). Complex **7g** gradually decomposed even at −10 °C and eventually gave an unidentifiable mixture, probably via the dissociation of the end-on CO ligand. A crystal suitable for the SC-XRD analysis was prepared from this resultant mixture by recrystallization at −30 °C, and we confirmed the presence of binuclear nickel carbonyl complex **8g** (Figure 4b).[43−46] Inspired by these results, we explored a possible mechanistic scenario for the formation of **7g** from **1g** and **B^1** based on DFT calculations at the PBE0-D3BJ/Def2-TZVPD//M06L/Def2-SVPD(Ni,F,O), Def2-SVP(others) level. The relative Gibbs free energies with respect to [**1g** + **B^1**] (0.0 kcal mol^{-1}) for selected molecules are shown in Figure 4b (for details, see Figure S29). We found that square-planar Ni complex **2g** (+8.0 kcal mol^{-1}), which bears **B^1** as a monodentate Z-type ligand, is formed via **TS1′** (+11.9 kcal mol^{-1}). While the Ni−B bond (2.43 Å) is longer than those in **2a**−**2c** (ca. 2.2 Å), the BCP found between these atoms by the AIM analysis supports the presence of the Ni → B interaction in **2g** (Figure S21). Moreover, as was seen for **2a**, the participation of multiple NCIs between the **L7** and **B^1** units in **2g** was confirmed. Subsequently, the Ni-to-C2 migration of **B^1** proceeds via **TS2′** (+23.9 kcal mol^{-1}) to yield **7g** (+1.6 kcal mol^{-1}). These results imply that the use of multidentate carbene ligands (e.g., **L1**−**L3**) that can generate FLP species with tris(perfluoroaryl)-boranes represents a strategy for generating transition metal complexes that bear monodentate Z-type borane ligands.

Based on the results obtained up to this point, we considered possible reaction mechanisms to afford **2a** from **1a** and **B^1**. Figure 5 depicts two selected paths with key intermediates and transition states (for further details, see Figure S28). Following the generation of association complex **Int1-v1** (+5.1 kcal mol^{-1}) from **1a** and **B^1**, the formation of the C2−B bond proceeds via **TS$_{add}$1** (+13.6 kcal mol^{-1}) to afford Ni(μ-η^1-CO)B species **Int2-v1** (+7.1 kcal mol^{-1}; C2−B 1.80 Å) (blue colored path). Subsequently, another CO ligand smoothly dissociates to yield **Int3-v1** (+12.1 kcal mol^{-1}) without a significant energy barrier, which eventually forms **Int4-v1** (+5.1 kcal mol^{-1}) via the complete removal of CO. Coordination of the C_{ip} atom in the C_6F_5 unit stabilizes **Int4-v1**, and the B atom effectively approaches the Ni center (Ni···B 2.31 Å). The C2-to-Ni migration of the B atom subsequently occurs via **TS$_{mig}$1** (+7.0 kcal mol^{-1}), resulting in the construction of the Ni−B bond (2.22 Å) together with the elongation of the C2···B distance to 2.41 Å from 1.78 Å in **Int4-v1**. This mechanistic scenario predicts the facile formation of **2a** after mixing **1a** and **B^1**, as the reaction rate would be predominantly determined by the formation of the C2−B bond via **TS$_{add}$1**, i.e., with an energy barrier of only +13.6 kcal mol^{-1}. In contrast, for **B^3** and **B^4**, the corresponding paths to form the C2−B bond and dissociate another CO ligand should become energetically unfavorable due to their decreased Lewis acidity, which would explain why no reaction was observed with **1a** (Figure 2). On the other hand, we also found that the formation of Ni(μ-η^1,η^2-CO)B species **Int2-v4**

https://doi.org/10.1021/jacs.4c15892
J. Am. Chem. Soc. 2025, 147, 8326−8335

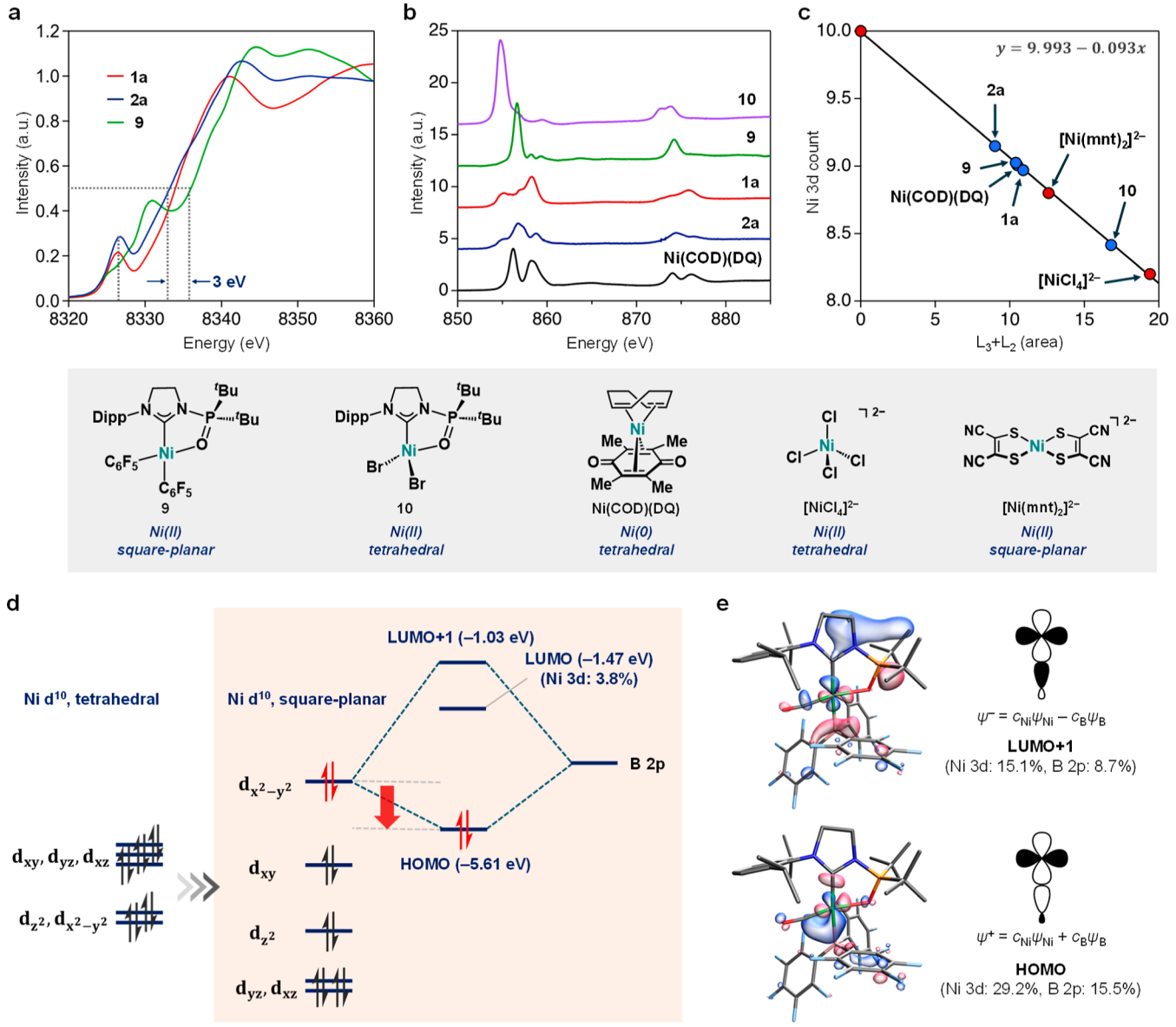

Figure 6. Experimental and theoretical evaluation of the electronic state of the Ni complexes examined in this study. (a) Ni K-edge XAS spectra. (b) Ni $L_{2,3}$-edge XAS spectra. (c) Sum-rule analysis. (d) A simplified Frontier-molecular-orbital energy diagram of **2a**, focusing on the interaction between the Ni and B centers, calculated at PBE0-D3BJ/Def2-TZVPD level. (e) Kohn−Sham HOMO and LUMO+1 in **2a** and their orbital composition.

(−1.6 kcal mol^{-1}) from **Int1-v1** via $\mathbf{TS_{ism}1}$ (+14.4 kcal mol^{-1}) can compete with the above pathway via $\mathbf{TS_{add}1}$ (gray colored path). The geometric parameters around the Ni atom in **Int2-v4** (e.g., Ni−C2 1.85 Å; Ni−O2 2.01 Å; C2−B 1.62 Å) are nearly identical to those in **7g** (Figure 4b), which bears **L4**, although the phosphinoyl O1 weakly coordinates to Ni in **Int2-v4**. This weak coordination of the phosphinoyl moiety should prevent the formation of a Ni−borane complex that bears two CO ligands and the carbene in **L1**, as seen in the interconversion between **2g** and **7g**. It would be possible to yield **2a** from **Int2-v4** via the regeneration of **Int1-v1** and then $\mathbf{TS_{mig}1}$ as a result of the change in the coordination mode of CO from a μ-η^1,η^2 to a μ-η^1 fashion; the overall energy barrier in this case is +16.0 kcal mol^{-1}. Conversely, the path directly connecting **Int2-v4** and **2a** is unfavorable due to the higher energy barrier to overcome $\mathbf{TS_{mig}2}$.

As mentioned earlier, the Ni center in **2a−c** and **3a** adopts a distorted square-planar geometry, which represents a fingerprint of the Ni(II) configuration in classical ligand-field theory. However, several transition metal complexes that bear Z-type ligands have been found to adopt unusual electronic configurations different from those expected based on their geometry.[47−51] Thus, we employed Ni K- and $L_{2,3}$-edge X-ray absorption spectroscopy (XAS) to gain insight into the electronic configuration of **2a**. Given that transition metal K-edge XAS is sensitive to the ligand-field geometry rather than the electronic state, we synthesized (κ-*C*,*O*-**L1**)Ni(C_6F_5)$_2$ (**9**), a low-spin square-planar nickel complex with the formal oxidation state +II, as a reference. The Ni K-edge X-ray absorption near edge structure (XANES) data are shown in Figure 6a. The absorption edge of **2a** appeared at 8333 eV with the pre-edge peak at 8327 eV; these values were almost identical to those of **1a**. In addition, the absorption edge of **9**

https://doi.org/10.1021/jacs.4c15892
J. Am. Chem. Soc. 2025, 147, 8326−8335

appeared at 8336 eV, i.e., 3 eV higher than that of **2a**. Considering the identical ligand-field geometries in **2a** and **9**, this edge-shift suggests that **2a** adopts the formal electric state Ni(0). The Ni $L_{2,3}$-edge XAS analysis afforded deeper insight, as the hole number in Ni 3d orbitals is proportional to the sum of the Ni L_3- and Ni L_2-edge peak area based on the sum rule.[52,53] To this end, Ni d-electron counts are inversely proportional to the sum of the Ni L_3- and Ni L_2-edge peak area, which allows transition metal $L_{2,3}$-edge XAS to be used as a direct probe for d-electron occupancy. The Ni $L_{2,3}$-edge XAS experiments were conducted using the total electron yield (TEY) method under vacuum conditions, and the obtained XAS data of the (*κ-C,O*-**L1**)Ni complexes **1a**, **2a**, **9**, and **10** are shown in Figure 6b, together with those of Ni(COD)(DQ) (COD: 1,5-cyclooctadiene, DQ: duroquinone).[54] For the formal Ni(II) complexes **9** (low-spin) and **10** (high-spin), sharp and intense L_3-edge peaks were observed at 856.6 and 854.8 eV, respectively. In contrast, Ni(COD)(DQ) exhibited a broadened first peak at 856.2 eV. A prominent second peak was detected at higher energy, which was ascribed to the Ni 2p → ligand transitions.[55] In the cases of **1a** and **2a**, the XAS signals are split into several peaks with low intensity, which was attributed to the influence of the electron-accepting ligands, such as carbonyl and borane. The Ni 3d electron counts were then calculated from the sum of the normalized peak area using the linear function established from the XAS data of the d-count calibrants $[Et_4N]_2[NiCl_4]$ and $[Na(benzo\text{-}15\text{-}crown\text{-}5)]_2[Ni(mnt)_2]$ (mnt: 1,2-dicyano-ethene-1,2-dithiolate) (Figure 6c and Table S6).[56,57] The Ni 3d count of **2a** (9.1) is comparable to those of the other formal Ni(0) complexes, such as **1a** (9.0) and Ni(COD)(DQ) (9.0). These results are also consistent with the estimated electron configuration of $(3d)^{9.10}(4s)^{0.32}$ calculated by the NBO7 program.

Finally, we disclose the role of tris(perfluoroaryl)boranes that contain *ortho*-F atoms, such as $\mathbf{B^1}$ and $\mathbf{B^2}$, in constructing the unusual square-planar geometry at the Ni(0) center with the occupied 3d electron configuration (Figure 6d). Based on ligand-field theory, Ni(0) d^{10} complexes usually adopt a tetrahedral geometry; this tendency is clearly observed in **6a** bearing *ortho*-protonated $\mathbf{B^5}$, which coordinates to the Ni center via the C_{ip} (labeled as C3 in Figure 3b). On the other hand, in the case of the $\mathbf{B^1}$/$\mathbf{B^2}$ ligands, the repulsive effects generated between the Ni and *ortho*-F atoms would prohibit such coordination of the C_{ip} atoms, and lead to orbital rehybridization to stabilize the high-lying occupied Ni $3d_{x^2-y^2}$ orbital with the assistance of *σ*-accepting $\mathbf{B^1}$/$\mathbf{B^2}$ ligands. As a result, **2a**−**c** and **3a** adopt sterically acceptable but electronically unfavorable square-planar geometries, i.e., the square-planar Ni $d^{9.1}$ state, where the electron density on the Ni center is modulated through interactions with the supporting ligands. In fact, DFT calculations showed that the HOMO and LUMO +1 in **2a** are predominantly located on the Ni−B bonds with significant contributions of the Ni 3d and B 2p atomic orbitals (HOMO: Ni 29.2% and B 15.5%; LUMO+1: Ni 15.1%, B 8.7%) (Figure 6e), supporting the conclusion that the Ni and B atoms form a typical Lewis base → acid interaction. Furthermore, an energy decomposition analysis (EDA) indicated a significant contribution of the electrostatic interaction (ΔE_{elstat}) in the stabilization of the square-planar Ni centers bearing $\mathbf{B^1}$ and $\mathbf{B^2}$ (Table S4).

CONCLUSIONS

In summary, we have isolated and fully characterized square-planar nickel carbonyl (Ni−CO) complexes that bear tris(perfluoroaryl)boranes as monodentate *σ*-accepting (Z-type) ligands. In these complexes, the Ni center exhibits a $d^{9.1}$ configuration with a high-lying occupied $3d_{x^2-y^2}$ orbital, which is effectively stabilized by the *σ*-accepting ability of tris(perfluoroaryl)boranes with *ortho*-F atoms. The Ni−B bonds in these complexes exhibit mixed covalent/dative character. In contrast, $B(3,5\text{-}(CF_3)_2C_6H_3)_3$ afforded a tetrahedral nickel complex via Ni−CO bond coordination to the boron atom, highlighting the critical role of the *ortho*-F atoms in constructing square-planar nickel−borane complexes. Under the explored experimental and theoretical conditions, such nickel−borane complexes seem to be generated through the combination of sterically encumbered *N*-heterocyclic carbenes (L-type ligands) and tris(perfluoroaryl)boranes (Z-type ligands). In addition, we observed the participation of multiple noncovalent interactions over the L−Ni−Z units, which should support the deformed tetrahedral four-coordinated boron units. This work thus demonstrates a strategy, namely, the use of frustrated L/Z-ligand pairs, for the formation of a hitherto elusive class of low-valent transition metal complexes.

ASSOCIATED CONTENT

Supporting Information

The Supporting Information is available free of charge at https://pubs.acs.org/doi/10.1021/jacs.4c15892.

Full details pertaining to the experimental methods, identification of the compounds, and DFT calculations (PDF)

AIM analysis (XLSX)

DFT coordinate (XLSX)

Accession Codes

Deposition Numbers 2384752−2384760 contain the supplementary crystallographic data for this paper. These data can be obtained free of charge via the joint Cambridge Crystallographic Data Centre (CCDC) and Fachinformationszentrum Karlsruhe Access Structures service.

AUTHOR INFORMATION

Corresponding Authors

Yuta Uetake − *Department of Applied Chemistry, Faculty of Engineering, Osaka University, Suita, Osaka 565-0871, Japan; Innovative Catalysis Science Division, Institute for Open and Transdisciplinary Research Initiatives (ICS-OTRI), Osaka University, Suita, Osaka 565-0871, Japan;* orcid.org/0000-0002-4742-8085; Email: uetake@chem.eng.osaka-u.ac.jp

Yoichi Hoshimoto − *Department of Applied Chemistry, Faculty of Engineering, Osaka University, Suita, Osaka 565-0871, Japan; Center for Future Innovation (CFi), Division of Applied Chemistry, Faculty of Engineering, Osaka University, Suita, Osaka 565-0871, Japan;* orcid.org/0000-0003-0882-6109; Email: hoshimoto@chem.eng.osaka-u.ac.jp

Authors

Yutaka Mondori − *Department of Applied Chemistry, Faculty of Engineering, Osaka University, Suita, Osaka 565-0871, Japan*

Yasuhiro Yamauchi − *Department of Applied Chemistry, Faculty of Engineering, Osaka University, Suita, Osaka 565-0871, Japan*

Takahiro Kawakita − *Department of Applied Chemistry, Faculty of Engineering, Osaka University, Suita, Osaka 565-0871, Japan*

Sensuke Ogoshi − *Department of Applied Chemistry, Faculty of Engineering, Osaka University, Suita, Osaka 565-0871, Japan;* orcid.org/0000-0003-4188-8555

Yasuo Takeichi − *Department of Applied Physics, Graduate School of Engineering, Osaka University, Suita, Osaka 565-0871, Japan;* orcid.org/0000-0003-3334-0274

Hidehiro Sakurai − *Department of Applied Chemistry, Faculty of Engineering, Osaka University, Suita, Osaka 565-0871, Japan; Innovative Catalysis Science Division, Institute for Open and Transdisciplinary Research Initiatives (ICS-OTRI), Osaka University, Suita, Osaka 565-0871, Japan;* orcid.org/0000-0001-5783-4151

Complete contact information is available at: https://pubs.acs.org/10.1021/jacs.4c15892

Notes

The authors declare no competing financial interest.

■ ACKNOWLEDGMENTS

We are grateful to Daisuke Hashizume (RIKEN) for insightful discussions on the AIM analysis. Ni K-edge XAS measurements were performed at the BL14B2 beamline of SPring-8 under the approval of the Japan Synchrotron Radiation Research Institute (proposal numbers 2020A1871, 2021A1630, 2022A1767, and 2022A1784). Ni $L_{2,3}$-edge XAS measurements were performed at the BL19B beamline of KEK under the approval of the Photon Factory Program Advisory Committee (proposal numbers 2022P013 and 2024G031), and at the BL4B beamline of the UVSOR Synchrotron Facility with the approval of the Institute for Molecular Science (proposal number 21-697). Parts of the theoretical calculations were performed using resources from the Research Center for Computational Science, Okazaki, Japan (24-IMS-C089). This project was supported by Grants-in-Aid for Transformative Research Area (A) Digitalization-driven Transformative Organic Synthesis (22H05363 to Y.H.); Green Catalysis Science for Renovating Transformation of Carbon-Based Resources (24H01851 to Y.U.); JSPS KAKENHI grant Scientific Research (C) (22K05095 to Y.U.); the JST FOREST Program (JPMJFR2222 to Y.H.); a JSPS Research Fellowship (to Y.Y.); and JST SPRING (to Y.M.).

■ REFERENCES

(1) Jensen, W. B. The Lewis Acid-Base Definitions: A Status Report. *Chem. Rev.* **1978**, *78*, 1−31.

(2) Crawley, M. L.; Trost, B. M. *Applications of Transition Metal Catalysis in Drug Discovery and Development: An Industrial Perspective*; John Wiley & Sons, 2012; ..

(3) Striegler, S.; Rieger, B.; Kacker, S.; Baugh, L. S. *Late Transition Metal Polymerization Catalysis*; Wiley VCH, 2003.

(4) Hartwig, J. F. *Organotransition Metal Chemistry: From Bonding to Catalysis*; University Science Books, 2010.

(5) Braunschweig, H.; Dewhurst, R. D.; Schneider, A. Electron-Precise Coordination Modes of Boron-Centered Ligands. *Chem. Rev.* **2010**, *110*, 3924−3957.

(6) Amgoune, A.; Bourissou, D. σ-Acceptor, Z-type ligands for transition Metals. *Chem. Commun.* **2011**, *47*, 859−871.

(7) Braunschweig, H.; Dewhurst, R. D. Transition metals as Lewis bases: "Z-type" boron ligands and metal-to-boron dative bonding. *Dalton Trans.* **2011**, *40*, 549−558.

(8) Bauer, J.; Braunschweig, H.; Dewhurst, R. D. Metal-Only Lewis Pairs with Transition Metal Lewis Bases. *Chem. Rev.* **2012**, *112*, 4329−4346.

(9) Parkin, G. Impact of the coordination of multiple Lewis acid functions on the electronic structure and v^n configuration of a metal center. *Dalton Trans.* **2022**, *51*, 411−427.

(10) Komuro, T.; Nakajima, Y.; Takaya, J.; Hashimoto, H. Recent progress in transition metal complexes supported by multidentate ligands featuring group 13 and 14 elements as coordinating atoms. *Coord. Chem. Rev.* **2022**, *473*, 214837−214864.

(11) Green, M. L. H. A new approach to the formal classification of covalent compounds of the elements. *J. Organomet. Chem.* **1995**, *500*, 127−148.

(12) Davydova, E. I.; Sevastianova, T. N.; Timoshkin, A. Y. Molecular complexes of group 13 element trihalides, pentafluorophenyl derivatives and Lewis superacids. *Coord. Chem. Rev.* **2015**, *297*, 91−126.

(13) Cowley, A. H. From group 13−group 13 donor−acceptor bonds to triple-decker cations. *Chem. Commun.* **2004**, 2369−2375.

(14) Burlitch, J. M.; Leonowicz, M. E.; Petersen, R. B.; Hughes, R. E. Coordination of Metal Carbonyl Anions to Triphenylaluminum, -gallium, and -indium and the Crystal Structure of Tetraethylammonium Triphenyl($(\eta^5$-Cyclopentadienyl)dicarbonyliron)aluminate-(Fe−Al). *Inorg. Chem.* **1979**, *18*, 1097−1105.

(15) Kameo, H.; Nakazawa, H. Saturated Heavier Group 14 Compounds as σ-Electron-Acceptor (Z-type) Ligands. *Chem. Rec.* **2017**, *17*, 268−286.

(16) For examples including Pt-complexes, see: Bauer, J.; Braunschweig, H.; Dewhurst, R. D.; Radacki, K. Reactivity of Lewis Basic Platinum Complexes Towards Fluoroboranes. *Chem.—Eur. J.* **2013**, *19*, 8797−8805.

(17) For examples including Fe-complexes, see: Burlitch, J. M.; Burk, J. H.; Leonowicz, M. E.; Hughes, R. E. Migration of triphenylboron from iron to a geminal η^5-cylopentadienyl ligand. *Inorg. Chem.* **1979**, *18*, 1702−1709.

(18) For examples including Rh-complexes, see: Alférez, M. G.; Moreno, J. J.; Gaona, M. A.; Maya, C.; Campos, J. Ligand Postsynthetic Functionalization with Fluorinated Boranes and Implications in Hydrogenation Catalysis. *ACS Catal.* **2023**, *13*, 16055−16066.

(19) Hashimoto, T.; Asada, T.; Ogoshi, S.; Hoshimoto, Y. Main group catalysis for H_2 purification based on liquid organic hydrogen carriers. *Sci. Adv.* **2022**, *8*, No. eade0189.

(20) Sakuraba, M.; Morishita, T.; Hashimoto, T.; Ogoshi, S.; Hoshimoto, Y. Remote Back Strain: A Strategy for Modulating the Reactivity of Triarylboranes. *Synlett* **2023**, *34*, 2187−2192.

(21) Hisata, Y.; Washio, T.; Takizawa, S.; Ogoshi, S.; Hoshimoto, Y. In-silico-assisted derivatization of triarylboranes for the ccatalytic reductive functionalization of aniline-derived amino acids and peptides with H_2. *Nat. Commun.* **2024**, *15*, 3708.

(22) Goedecke, C.; Hillebrecht, P.; Uhlemann, T.; Haunschild, R.; Frenking, G. The Dewar-Chatt-Duncanson model reversed: Bonding analysis of group-10 complexes $[(PMe_3)_2M{-}EX_3]$ (M = Ni, Pd, Pt; E = B, Al, Ga, In, Tl; X = H, F, Cl, Br, I). *Can. J. Chem.* **2009**, *87*, 1470−1479.

(23) Erdmann, P.; Greb, L. What Distinguishes the Strength and the Effect of a Lewis Acid: Analysis of the Gutmann−Beckett Method. *Angew. Chem., Int. Ed.* **2022**, *61*, No. e202114550.

(24) For examples including Ru-complexes, see: Hill, A. F.; Owen, G. R.; White, A. J. P.; Williams, D. J. The Sting of the Scorpion: A Metallaboratrane. *Angew. Chem., Int. Ed.* **1999**, *38*, 2759−2761.

(25) Hill, A. F. An Unambiguous Electron-Counting Notation for Metallaboratranes. *Organometallics* **2006**, *25*, 4741−4743.

(26) For examples including Rh-complexes, see: Crossley, I. R.; Hill, A. F.; Willis, A. C. Metallaboratranes: Tris(methimazolyl)borane Complexes of Rhodium(I). *Organometallics* **2006**, *25*, 289−299.

(27) Parkin, G. A. Simple Description of the Bonding in Transition-Metal Borane Complexes. *Organometallics* **2006**, *25*, 4744−4747.
(28) For examples including Ni-, Cu-, Pd-, Ag-, Pt- and Au-complexes, see: Sircoglou, M.; Bontemps, S.; Bouhadir, G.; Saffon, N.; Miqueu, K.; Gu, W.; Mercy, M.; Chen, C.-H.; Foxman, B. M.; Maron, L.; Ozerov, O. V.; Bourissou, D. Group 10 and 11 Metal Boratranes (Ni, Pd, Pt, CuCl, AgCl, AuCl, and Au^+) Derived from a Triphosphine−Borane. *J. Am. Chem. Soc.* **2008**, *130*, 16729−16738.
(29) For examples including Ni- and Pd-complexes, see: Emslie, D. J. H.; Harrington, L. E.; Jenkins, H. A.; Robertson, C. M.; Britten, J. F. Group 10 Transition-Metal Complexes of an Ambiphilic PSB-Ligand: Investigations into η^3(BCC)-Triarylborane Coordination. *Organometallics* **2008**, *27*, 5317−5325.
(30) For examples including Ni-complexes, see: Harman, W. H.; Peters, J. C. Reversible H_2 Addition across a Nickel-Borane Unit as a Promising Strategy for Catalysis. *J. Am. Chem. Soc.* **2012**, *134*, 5080−5082.
(31) Stephan, D. W.; Erker, G. Frustrated Lewis Pair Chemistry: Development and Perspectives. *Angew. Chem., Int. Ed.* **2015**, *54*, 6400−6441.
(32) Jupp, A. R.; Stephan, D. W. New Directions for Frustrated Lewis Pair Chemistry. *Trends Chem.* **2019**, *1*, 35−48.
(33) Yamauchi, Y.; Mondori, Y.; Uetake, Y.; Takeichi, Y.; Kawakita, T.; Sakurai, H.; Ogoshi, S.; Hoshimoto, Y. Reversible Modulation of the Electronic and Spatial Environment around Ni(0) Centers Bearing Multifunctional Carbene Ligands with Triarylaluminum. *J. Am. Chem. Soc.* **2023**, *145*, 16938−16947.
(34) Carden, J. L.; Dasgupta, A.; Melen, R. L. Halogenated triarylboranes: synthesis, properties and applications in catalysis. *Chem. Soc. Rev.* **2020**, *49*, 1706−1725.
(35) Ashley, A. E.; Herrington, T. J.; Wildgoose, G. G.; Zaher, H.; Thompson, A. L.; Rees, N. H.; Krämer, T.; O'hare, D. Separating Electrophilicity and Lewis Acidity: The Synthesis, Characterization, and Electrochemistry of the Electron Deficient *Tris*(aryl)boranes $B(C_6F_5)_{3-n}(C_6Cl_5)_n$ (n = 1−3). *J. Am. Chem. Soc.* **2011**, *133*, 14727−14740.
(36) Sakuraba, M.; Hoshimoto, Y. Recent Trends in Triarylborane Chemistry: Diversification of Structures and Reactivity via *meta*-Substitution of the Aryl Groups. *Synthesis* **2024**, *56*, 3421.
(37) Braunschweig, H.; Dewhurst, R. D.; Gessner, V. H. Transition metal borylene complexes. *Chem. Soc. Rev.* **2013**, *42*, 3197−3208.
(38) Kong, L.; Lu, W.; Yongxin, Y.; Ganguly, R.; Kinjo, R. Formation of Boron−Main-Group Element Bonds by Reactions with a Tricoordinate Organoboron L_2PhB: (L = Oxazol-2-ylidene). *Inorg. Chem.* **2017**, *56*, 5586−5593.
(39) Reineke, M. H.; Sampson, M. D.; Rheingold, A. L.; Kubiak, C. P. Synthesis and Structural Studies of Nickel(0) Tetracarbene Complexes with the Introduction of a New Four-Coordinate Geometric Index, $\tau\delta$. *Inorg. Chem.* **2015**, *54*, 3211−3217.
(40) Holschumacher, D.; Bannenberg, T.; Hrib, C. G.; Jones, P. G.; Tamm, M. Heterolytic Dihydrogen Activation by a Frustrated Carbene-Borane Lewis Pair. *Angew. Chem., Int. Ed.* **2008**, *47*, 7428−7432.
(41) Chase, P. A.; Stephan, D. W. Hydrogen and Amine Activation by a Frustrated Lewis Pair of a Bulky N-Heterocyclic Carbene and $B(C_6F_5)_3$. *Angew. Chem., Int. Ed.* **2008**, *47*, 7433−7437.
(42) Choukroun, R.; Lorber, C.; Lepetit, C.; Donnadieu, B. Reactivity of $[Cp_2Ti(CO)_2]$ and $B(C_6F_5)_3$: Formation of the Acylborane Complexes $[Cp_2Ti(CO)(\eta^2\text{-}OCB(C_6F_5)_3)]$ and $[Cp_2Ti(THF)(\eta^2\text{-}OCB(C_6F_5)_3)]$. *Organometallics* **2003**, *22*, 1995−1997.
(43) Lyngdoh, R. H. D.; Schaefer, H. F.; King, R. B. Metal-Metal (MM) Bond Distances and Bond Orders in Binuclear Metal Complexes of the First Row Transition Metals Titanium Through Zinc. *Chem. Rev.* **2018**, *118*, 11626−11706.
(44) Shriver, D. F. BASCITY AND REACTIVITY OF METAL CARBONYLS. *J. Organomet. Chem.* **1975**, *94*, 259−271.
(45) Gong, J.-K.; Kubiak, C. P. A New Route to the Ni(0) 'Cradle' Complex $Ni_2(\mu\text{-}CO)(CO)_2(PPh_2CH_2PPh_2)_2$: μ-CO Ligand and Metal-centered Reactivity. *Inorg. Chim. Acta* **1989**, *162*, 19−21.
(46) Bernhardt, E.; Finze, M.; Willner, H.; Lehmann, C. W.; Aubke, F. Salts of the Cobalt(I) Complexes $[Co(CO)_5]^+$ and $[Co(CO)_2(NO)_2]^+$ and the Lewis Acid-Base Adduct $[Co_2(CO)_7CO\text{-}B(CF_3)_3]$. *Chem.—Eur. J.* **2006**, *12*, 8276−8283.
(47) Wade, C. R.; Lin, T.-P.; Nelson, R. C.; Mader, E. A.; Miller, J. T.; Gabbaï, F. P. Synthesis, Structure, and Properties of a T-shaped 14-Electron Stiboranyl-Gold Complex. *J. Am. Chem. Soc.* **2011**, *133*, 8948−8955.
(48) Ansmann, N.; Münch, J.; Schorpp, M.; Greb, L. Neutral and Anionic Square Planar Palladium(0) Complexes Stabilized by a Silicon Z-Type Ligand. *Angew. Chem., Int. Ed.* **2023**, *62*, No. e202313636.
(49) For examples including Pt-complexes, see: Kameo, H.; Tanaka, Y.; Shimoyama, Y.; Izumi, D.; Matsuzaka, H.; Nakajima, Y.; Lavedan, P.; Le Gac, A.; Bourissou, D. Square-Planar Anionic Pt^0 Complexes. *Angew. Chem., Int. Ed.* **2023**, *62*, No. e202301509.
(50) Wächtler, E.; Gericke, R.; Block, T.; Pöttgen, R.; Wagler, J. Trivalent Antimony as L-, X-, and Z-Type Ligand: The Full Set of Possible Coordination Modes in Pt-Sb Bonds. *Inorg. Chem.* **2020**, *59*, 15541−15552.
(51) For examples including Au-complexes, see: Sircoglou, M.; Bontemps, S.; Mercy, M.; Saffon, N.; Takahashi, M.; Bouhadir, G.; Maron, L.; Bourissou, D. Transition-Metal Complexes Featuring Z-Type Ligands: Agreement or Discrepancy between Geometry and d^n Configuration? *Angew. Chem., Int. Ed.* **2007**, *46*, 8583−8586.
(52) Dimucci, I. M.; Lukens, J. T.; Chatterjee, S.; Carsch, K. M.; Titus, C. J.; Lee, S. J.; Nordlund, D.; Betley, T. A.; MacMillan, S. N.; Lancaster, K. M. The Myth of d^8 Copper(III). *J. Am. Chem. Soc.* **2019**, *141*, 18508−18520.
(53) DiMucci, I. M.; Titus, C. J.; Nordlund, D.; Bour, J. R.; Chong, E.; Grigas, D. P.; Hu, C. H.; Kosobokov, M. D.; Martin, C. D.; Mirica, L. M.; Nebra, N.; Vicic, D. A.; Yorks, L. L.; Yruegas, S.; MacMillan, S. N.; Shearer, J.; Lancaster, K. M. Scrutinizing Formally Ni^{IV} centers through the lenses of core spectroscopy, molecular orbital theory, and valence bond theory. *Chem. Sci.* **2023**, *14*, 6915−6929.
(54) Tran, V. T.; Li, Z. Q.; Apolinar, O.; Derosa, J.; Joannou, M. V.; Wisniewski, S. R.; Eastgate, M. D.; Engle, K. M. Ni(COD)(DQ): An Air-Stable 18-Electron Nickel(0)-Olefin Precatalyst. *Angew. Chem., Int. Ed.* **2020**, *59*, 7409−7413.
(55) Hatsui, T.; Kosugi, N. Metal-to-ligand charge transfer in polarized metal L-edge X-ray absorption of Ni and Cu Complexes. *J. Electron Spectrosc. Relat. Phenom.* **2004**, *136*, 67−75.
(56) Solomon, E. I.; Hedman, B.; Hodgson, K. O.; Dey, A.; Szilagyi, R. K. Ligand K-Edge X-ray aabsorption spectroscopy: covalency of ligand-metal bonds. *Coord. Chem. Rev.* **2005**, *249*, 97−129.
(57) Sarangi, R.; George, S. D. B.; Rudd, D. J.; Szilagyi, R. K.; Ribas, X.; Rovira, C.; Almeida, M.; Hodgson, K. O.; Hedman, B.; Solomon, E. I. Sulfur K-Edge X-ray Absorption Spectroscopy as a Probe of Ligand-Metal Bond Covalency: Metal vs Ligand Oxidation in Copper and Nickel Dithiolene Complexes. *J. Am. Chem. Soc.* **2007**, *129*, 2316−2326.

https://doi.org/10.1021/jacs.4c15892
J. Am. Chem. Soc. 2025, 147, 8326−8335